

Journal of Astronomical Telescopes, Instruments, and Systems

AstronomicalTelescopes.SPIEDigitalLibrary.org

On the in-flight calibration plans of modern x-ray observatories

Matteo Guainazzi
Laurence David
Catherine E. Grant
Eric Miller
Lorenzo Natalucci
Jukka Nevalainen
Robert Petre
Marc Audard

On the in-flight calibration plans of modern x-ray observatories

Matteo Guainazzi,^{a,b,*} Laurence David,^c Catherine E. Grant,^d Eric Miller,^d Lorenzo Natalucci,^e Jukka Nevalainen,^f Robert Petre,^g and Marc Audard^h

^aESA-European Space Astronomy Centre, Villafranca del Castillo, Madrid E-28692, Spain

^bInstitute of Space and Astronautical Science, Japan Aerospace Exploration Agency, 3-1-1 Yoshinodai, Chuo-ku, Sagami-hara, Kanagawa 252-5210, Japan

^cHarvard-Smithsonian Center for Astrophysics, 60 Garden Street, Cambridge, Massachusetts 02138, United States

^dKavli Institute for Astrophysics and Space Research, Massachusetts Institute of Technology, 77 Massachusetts Avenue, Cambridge, Massachusetts 02139-4307, United States

^eIstituto Nazionale di Astrofisica, INAF-IAPS, via del Fosso del Cavaliere, I-00133 Roma, Italy

^fTartu Observatory, Toravere 61602, Estonia

^gNASA, Goddard Space Flight Center, Greenbelt, Maryland 20771, United States

^hUniversity of Geneva, Department of Astronomy, Chemin d'Ecogia 16, Versoix 1290, Switzerland

Abstract. We present an overview of the set of celestial sources used for in-flight calibration of x-ray detectors by past and operational missions. We show the rationale behind their choice as a guideline for future missions aiming at optimizing the critical early phases of their science operations. © 2015 Society of Photo-Optical Instrumentation Engineers (SPIE) [DOI: [10.1117/1.JATIS.1.4.047001](https://doi.org/10.1117/1.JATIS.1.4.047001)]

Keywords: x-ray instrumentation; operations; x-rays.

Paper 15054 received Jun. 21, 2015; accepted for publication Nov. 17, 2015; published online Dec. 29, 2015.

1 Art of Calibrating X-Ray Instruments

Ideally, calibration of space x-ray instruments is the result of a complete physical model supported by an adequate set of ground-based measurements under controlled conditions. Regrettably, time and budget pressure during the mission development phase, as well as the degradation of the instrument performance in space (radiation damage, contamination, electronic failures, and degrading thermal environment) more often than not require recalibration using celestial sources. “In-flight” calibration programs have been playing a crucial role in our understanding of the instruments’ scientific performance, as well as (and, often, more crucially) of their time evolution.

While x-ray astronomy is nowadays a fully mature and globally integrated science, a wide variety of approaches in dealing with similar calibration issues has been developed by different missions, and, a variety of celestial sources has been used for the same calibration purpose. Moreover, the suitability of a celestial source for calibration purposes depends on the commensurability between observables related to the intrinsic astrophysical properties and instrument performance. For instance, thermal or velocity broadening of emission line profiles has a negligible impact on the calibration or energy scale and line spread function (LSF) at charge-coupled device (CCD) resolution ($E/\Delta E \sim 10$), while they must be taken into account at grating or calorimeter resolution ($E/\Delta E \gtrsim 10^2$).

The International Astronomical Consortium for High-Energy Calibration (IACHEC)¹, was inaugurated in 2006 to foster a better integration among calibration activities of operational high-energy observatories. In this context, the IACHEC aims

to provide standards for high-energy calibration and coordinate cross-calibration between different missions. This goal is reached through working groups, where IACHEC members cooperate to define calibration standards and procedures. The scope of these groups is primarily a practical one: a set of data and results (eventually published in refereed journals) will be the outcome of a coordinated and standardized analysis of reference sources (“high-energy standard candles”). Past, present, and future high-energy missions can then use these results as a calibration reference. In this context, one of the goals of IACHEC is to develop a web-based archive of calibrated data sets, spectral models, and response files for all “standard candles” from all high-energy missions. This suite of calibrated data sets can then be used to ensure a proper cross-calibration. Another goal of the IACHEC is providing future missions with a test-bed of consolidated experiences and good practices that can be beneficial in designing and optimizing in-flight calibration plans.

Regrettably, calibration of x-ray astronomy instrumentation cannot rely on “standard candles” *strictu sensu*, i.e., on sources whose absolute flux and spectrum are known once other astrophysical observables are measured. One must be content with sources for which an educated guess of the physical process responsible for their x-ray emission is available. These “x-ray standard candles” exhibit nonthermal broadband spectra or thermal spectra in the soft x-ray band ($\lesssim 2$ keV). For each source in this set of “x-ray standard candles,” the IACHEC aims to define data reduction and analysis procedures, and a reference astrophysical model, and to publish these ideally in refereed journals.

In this paper, we present the main celestial objects employed in the in-flight calibration plans of all the missions active in the IACHEC context (basically, all the operational x-ray observatories from the 1990s of the past century to now). Our primary

*Address all correspondence to: Matteo Guainazzi; E-mail: Matteo.Guainazzi@sciops.esa.int

This paper was written in the framework of the activities of the IACHEC Heritage Working Group.

goal is providing a reference that might be used by future missions to optimize the preparation of their calibration operations after launch. Discussing the results of the calibration experiments or the level of accuracy achieved with them is beyond the scope of this paper. Readers interested in these aspects are referred to the list of references in [Appendix A](#) of this paper.

X-ray astronomy is significantly older (and wiser) than the arbitrary time threshold applied to the missions covered by this paper. Reconstructing the quality and the accuracy of calibration measurements for older missions is often hard. Their data have not always been adequately preserved. While old archival data still contain excellent, and partly still uncovered science, we decided to discuss in this paper only those past and operational missions whose calibration results have been discussed, and to a certain extent “validated” through the common work at the IACHEC. This choice introduces an historical bias in our synopsis, of which we, the authors, are well aware.

In this paper, we summarize the primary calibration sources used for the in-flight calibration of the following items: “high-resolution” line spread function (LSF) and wavelength scale in [Sec. 2](#); redistribution, resolution, and energy scale in x-ray CCDs in [Sec. 3](#); effective area in [Sec. 4](#) and [Sec. 5](#); point spread function (PSF) in [Sec. 6](#); accuracy of event time assignment in [Sec. 7](#); and instrumental cross-calibration in [Sec. 8](#). In the [Appendix](#), we list the instruments discussed in this paper. While the background affects the analysis of calibration and science observations likewise and stacking of diffuse background can be regarded as a fundamental calibration product, we do not discuss background calibration in this paper.

2 High-Resolution Line Spread Function and Wavelength Scale

Spectra of x-ray bright cool stars have been used for the calibration of the LSF (The LSF is the response to a monochromatic emission line in energy/wavelength space.) and wavelength scale in the Chandra/low-energy transmission grating (LETG) and high-energy transmission grating (HETG) and the XMM-Newton/RGS ([Table 1](#)): ABDor, Algol, Capella, HR1099, and Procyon. Their x-ray spectrum is due to coronal emission, with temperatures of a few MK, and soft x-ray fluxes $\sim 10^{-10}$ erg cm $^{-2}$ s $^{-1}$ in the ROSAT band (0.1 to 2.4 keV)² ([Fig. 1](#)). Capella is on the average of the brightest and the least variable in this sample; its historical RGS light curve exhibits a dynamical range of $\pm 15\%$, as well as excess fluctuations over those expected from pure Poissonian noise at the 2% to 7% level on time scales as short as a few hours.³ ABDor and HR1099 exhibit large flaring activities, with flux changes of up to 1 order of magnitude on time scales as short as a few hours.^{4,5} This prevents them from being used for absolute flux calibration of their line intensities. However, no variation of the observables

Table 1 Main sources used for the calibration of the LSF and wavelength scale in high-resolution detectors.

Source	LETG	HETG	RGS
Capella	X	X	X
HR1099		X	X
Procyon	X		X

on which the LSF and wavelength scale calibration depends has been reported so far.

The spectrum of some of these stars (Capella, most notably) is too soft to adequately cover the whole x-ray spectral bandpass. This is particularly important for the future calibration of the microcalorimeter on-board ASTRO-H (soft x-ray spectrometer, SXS⁶) at the astrophysically crucial iron atomic transitions at 6 to 7 keV. HR1099 and ABDor are sufficiently hot for this purpose, but the thermal broadening of emission lines must be taken into account, potentially complicating the measurement of the instrumental properties. Alternatively, Fe-K fluorescence lines are commonly observed, for instance, in the spectra of x-ray binaries (XRB). In particular, there exists a population of heavily obscured XRBs whose Fe line exhibits a very large (keV) equivalent width (EW). Among the best-studied (and brightest) examples of this sample are IGRJ16318-4848⁷ and GX301-2.⁸ Their lines are unresolved at the Chandra/HETG resolution. However, curve-of-growth analysis and other considerations are compatible with these lines being produced in the wind of the OB companion.⁹ The Chandra upper limit on the width is 770 km/s, while the value stemming from terminal velocity of the star wind is 850 km/s, corresponding to ≈ 18 eV full width half maximum at the energy of the resonant transition of He-like iron (Fe_{XXV}). More importantly, lines produced in stellar wind may have a complex structure with red wings.¹⁰ For these reasons, it is, therefore, unclear yet if these sources could be used for the calibration of LSF and energy scale in detectors with an eV-like resolution, like the SXS.

3 Charge-Coupled Device Redistribution, Resolution, and Energy Scale

The operation of x-ray CCDs differs from those in the optical band in that each detected x-ray photon produces a charge cloud related to the energy of the photon. These charge packets are collected over some short integration time before being read out and processed into events by the instrument electronics. Ideally the amount of charge in each packet would be directly proportional to the incoming photon energy with a small dispersion (the spectral resolution), but in practice several processes can redistribute events to measured energies well away from the expectation. Some of these processes are related to the photon-CCD interaction (Si escape and fluorescence peaks, constant low-energy shelves from charge lost in a noninteracting substrate, and pileup from multiple x-rays landing in the same region of the CCD); some are caused by the transfer of charge unique to CCDs (charge transfer efficiency or CTI); and some are caused by the electronic read-out (gain drift). Dark currents can add charge to cells. This energy redistribution, along with the efficiency of the telescope, filters, and detectors themselves, produces what is referred to as the “response” of an x-ray instrument to a photon of a given energy. Each of the aforementioned features may change with either temperature or radiation environment, requiring their monitoring over the mission and during each individual observation. (A full description of the operation of an x-ray CCD is beyond the scope of this work, and the reader is referred to Chapter 3 of the “Handbook of X-ray Astronomy.”¹¹)

While the redistribution shape can, in principle, be adequately characterized by illuminating the cameras with monochromatic beams on the ground, various forms of radiation damage in orbit produce spectral degradation. The resultant increase in CTI has required a recalibration of the photon

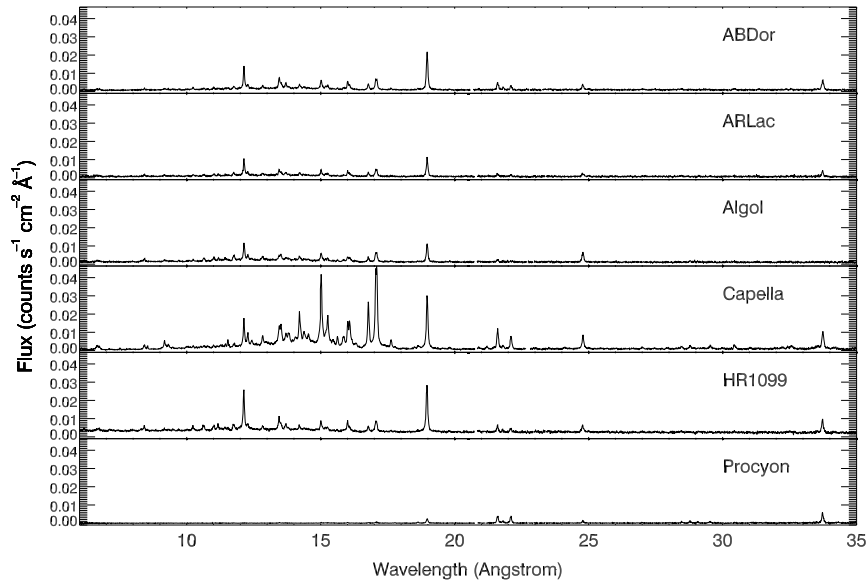


Fig. 1 RGS spectra from the longest XMM-Newton observation of six cool stars used for the calibration of the LSF and wavelength scale to illustrate their relative intensity. The spectra are displayed on the same y-axis linear scale to ease comparison.

redistribution alongside the energy scale (or gain) in several space x-ray CCDs. Characterization of the CTI requires uniform illumination of the whole CCD with a source of known spectrum, ideally with well-isolated (at CCD resolution) atomic transitions. In the XMM-Newton/EPIC cameras, a specific position of the filter wheel (CAL_CLOSED) allows an ^{55}Fe source [^{55}Fe decays by electron capture to ^{55}Mn , and the K-shell vacancy left by the process is filled by emitting Auger electrons, a Mn K_{α} doublet (~ 5.9 keV) and a Mn K_{β} singlet (~ 6.5 keV). L-shell lines, generally shielded by design, were allowed to shine through onto the ACIS detector, and were used for contamination monitoring during the early phase of the Chandra mission. Fluorescent targets may add additional lines such as Al K_{α} (~ 1.5 keV), Ti K_{α} (~ 4.5 keV), and Ti K_{β} (~ 4.9 keV).] to illuminate the whole field-of-view. Similarly, an ^{55}Fe source illuminates the ACIS field-of-view when it is transferred into the stowed position before and after each passage through the radiation belts. The Suzaku/XIS and the Swift/XRT also make use of ^{55}Fe calibration sources which permanently illuminate small regions of the CCDs; however, these are only sufficient to verify CTI corrections or monitor changes, not to properly measure the CTI across the detector. In addition, the ^{55}Fe source has a half-life time of only 2.7 years, a potential issue for long-lasting missions such as Chandra or XMM-Newton. The decreasing source flux, the different illumination conditions when compared with a typical astronomical background, the limited spectral range where the ^{55}Fe produces atomic transitions, and the lack of field-filling calibration sources in some missions complicate CTI measurements using on-board sources alone. (Recently, “modulated x-ray sources” have been designed whose x-ray source is pulsed. This allows a continuous monitoring of the energy scale over the whole field-of-view during astronomical observations by selecting only the short intervals where the pulses occur. The background is, therefore, not increased during scientific observations. Modulated x-ray sources have been installed on the SXS microcalorimeter on board ASTRO-H.¹²) These limitations require complementary observations of extended celestial sources with strong and well-isolated (at

CCD resolution) atomic transitions. A list of the main targets used for this purpose is given in Table 2.

Historically, supernova remnants (SNRs) have been the primary choice due to their: (a) extended emission covering the entirety or at least a large fraction of the field-of-view, and; (b) thermal spectrum, rich with emission lines that can be used as an absolute reference for the calibration of the energy scale, and whose physics can be understood at a level of precision sufficient for calibration purposes as being due to an optically thin collisionally ionized plasma, characterized by its temperature kT and its cosmic abundance. Cassiopeia A (Cas A) ($6' \times 6'$; 0.3 to 10 keV flux $\sim 2.5 \times 10^{-9}$ erg cm^{-2} s^{-1} ; kT ~ 0.6 to 4 keV) was the official first-light target for Chandra,

Table 2 Main sources used for the calibration of CTI, gain, and redistribution in CCD x-ray detectors.

Source	ACIS	EPIC-MOS	EPIC-pn	XIS	XRT
1E0102-72	X	X	X	X	X
3C273		X			X
CasA	X	X	X		X
Cygnus Loop				X	
Perseus cluster		X		X	
PKS2155-304		X			X
RXJ1856.5-3754		X			X
Tycho SNR		X	X		X
Vela SNR			X		
ζ Puppis		X	X		
ζ Orionis		X	X		

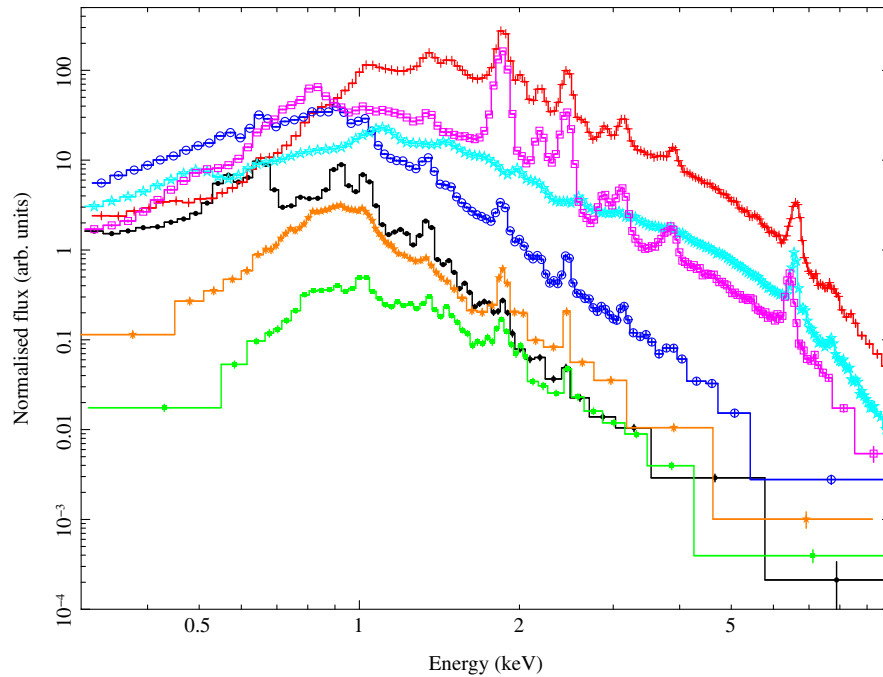


Fig. 2 EPIC-MOS1 spectra of SNR and galaxy clusters used for CCD redistribution calibration to illustrate their relative intensities. In order of decreasing flux at 0.4 keV: N132D (empty circles); Perseus Clusters (innermost 2'; empty stars); Cassiopeia A (crosses); Tycho (empty squares); 1E0102-72 (filled circles); N103B (filled stars); IC443 (filled squares).

primarily because it is bright, has many well-separated spectral features up to Fe, and is matched in size to an ACIS CCD. However, it is also absorbed less than 1 keV, i.e., close to the peak of the telescope effective area. The vela SNR is a huge structure ($\sim 8' \times 8'$), extensively used by the EPIC calibration team to calibrate the readout losses. Large-scale SNRs as the Cygnus Loop (≈ 3 deg; 0.3 to 10 keV flux $\sim 2.5 \times 10^{-10}$ erg cm $^{-2}$ s $^{-1}$; kT ~ 0.2 keV), Puppis A ($50' \times 60'$; 0.3 to 8 keV flux $\sim 2 \times 10^{-8}$ erg cm $^{-2}$ s $^{-1}$), galaxy clusters such as the Perseus cluster (~ 1 deg; 0.3 to 10 keV flux $\sim 2 \times 10^{-10}$ erg cm $^{-2}$ s $^{-1}$; kT ~ 3.5 keV) or the diffuse emission surrounding the Galactic Center were used by Suzaku/XIS for CTI measurements. The characterization of transfer losses in the central area of the Swift/XRT made use of compact x-ray bright SNR such as Cas A, IC443 ($2.2' \times 1.3'$; 0.3 to 10 keV flux $\sim 5 \times 10^{-12}$ erg cm $^{-2}$ s $^{-1}$), or Tycho ($8.7' \times 8.6'$; 0.3 to 10 keV flux $\sim 5 \times 10^{-10}$ erg cm $^{-2}$ s $^{-1}$; kT ~ 1 to 10 keV). Tycho is also one of the targets used to characterize transfer losses in the EPIC-MOS. A compilation of EPIC-MOS count spectra in the 0.3 to 10 keV energy band is shown in Fig. 2 to provide readers with a gauge of their relative intensity.

Studying the spectral resolution and redistribution and its evolution in space also requires bright sources with well-isolated (at CCD resolution) atomic transitions. The most used and studied source in the IACHEC context is the compact SNR 1E0102-72.3¹³ ($\approx 1'$ diameter; 0.3 to 10 keV flux $\sim 6 \times 10^{-11}$ erg cm $^{-2}$ s $^{-1}$; kT $\sim 0.2 - 0.5$ keV). The combination of symmetric morphology, lack of Fe-L lines, strong and well-isolated OVII, OVII, NeIX, and NeX emission lines, detailed empirical and astrophysical modeling, and deep available observations with all major operational CCD in space (together with a flux constant at a level of better than 1% in all knots)¹⁴ make 1E0102-72.3 a widely used “standard candle” in soft x-ray astronomy.¹⁵ Stars like ζ Puppis and ζ Orionis offer alternatively

strong NV lines. Very soft continuum sources such as the isolated neutron star (INS) RXJ1856.6-3754 offer complementary information due to their simple blackbody-like spectrum,¹⁶ and—at least for the latter source—extreme stability.¹⁷ Additional calibration of the redistribution can be achieved by looking at the agreement between data and models in bright power-law sources at energy ranges where the effective area exhibits the steepest gradients. Galactic black hole binaries such as LMCX-3 or radio-loud active galactic nuclei (AGN) such as 3C273¹⁸ and PKS2155-304¹⁹ have been used for this purpose. These same sources have also been used by ACIS to calibrate the energy scale at low energies ($\lesssim 500$ eV) using gratings observations.

4 Effective Area at Energies <10 keV

In optical astronomy, there are many stable point sources (mostly stars) with a range of colors that can be used as standard candles. While there are stable point sources in the energies lower than 1 keV (e.g., white dwarfs and INSs), there are no known stable point sources in the medium x-ray band (2 to 10 keV). For this reason, extended sources (e.g., SNR and clusters of galaxies) are commonly used as standard candles in this band. In addition, only faint point sources can be used to prevent pileup effects in CCDs, while gratings observations of extended sources are excluded to prevent degradation in the spectral resolution.

4.1 Compact Sources

The most commonly used sources for the in-flight calibration of the soft x-ray effective area are largely coincident with those used for the calibration of the redistribution (Table 3). Those effects can be hard to disentangle, especially in the softest energy bandpass of x-ray CCDs, where the energy resolving power significantly degrades.²⁰ The compact SNR 1E0102-72.3

Table 3 Main sources used for the calibration of the effective area below 10 keV.

Source	HRC	LETG	HETG	RGS	ACIS	EPIC-MOS	EPIC-pn	GSC	SSC	JEM-X	PCA	XIS	XRT
1E0102-72					X	X						X	X
3C273		X	X										X
Abell1795					X	X	X						
Abell2029					X	X	X					X	
Bright Earth limb												X	
Cygnus Loop												X	
Coma cluster					X	X	X					X	
Crab Nebula				X				X	X	X	X		X
G21.5-0.9	X				X								X
H1426+428			X										X
HZ43	X	X											
Mkn421	X	X	X	X	X ^a								X
Perseus cluster						X	X						
PKS2155-304	X	X	X	X	X ^a							X	
RXJ1856.5-3754		X		X								X	X

^aObservations done with a combination gratings + detector.

has been extensively used for this purpose.¹⁵ Very soft INS (RXJ1856.6-3754) and white dwarfs such as Sirius B, GD153 or HZ43 exhibit a blackbody-like spectrum with an effective temperature in the range 30 to 70×10^5 K and low photoelectric absorption column densities ($N_H \lesssim 10^{20}$ cm⁻²), making them appropriate sources to calibrate the effective area in the soft x-ray band.²¹ Extended long-term monitoring with all the major modern x-ray satellites confirmed that the x-ray emission of 1E0102-72 and RXJ1856-3754 is constant within a few percent over one decade,^{15,17} at variance with Cas A.²²

In the 2 to 10 keV band, radio-loud AGN with relative featureless spectra, such as 3C273, H1426+128, and PKS2155-304, are still widely used for effective area calibration. Their x-ray emission is believed to be dominated by a relativistic jet seen at a very small angle from the line-of-sight, although the decomposition of the 3C273 spectrum might be more complex and a variable contribution from the thermal accretion disk cannot be ruled out.^{23,24} Their nonthermal emission is dominated by either synchrotron or inverse Compton-scattering of the cosmic microwave background, well described by a power-law with a single photon index, or a slowly varying index with energy.²⁵

Table 4 Sources used for the calibration of the effective area above 10 keV.

Source	AGILE	BAT	HXD	HEXTE	IBIS	NuSTAR
Crab Nebula	X ^a	X	X	X	X	X
PSR1509-58			X		X	

^aCrab pulsar.

Objects used for calibration purposes exhibit fluxes of the order of several mCrab. (We assume here $1 \text{ mCrab} \equiv 2 \times 10^{-11}$ erg cm⁻² s⁻¹ in the 2 to 10 keV energy band.) A cross-calibration campaign on PKS2155-304 (now involving Chandra, NuSTAR, Suzaku, Swift, and XMM-Newton) has been running continuously since 2006,¹⁹ with one observation every year. However, radio-loud AGN, and in particular blazars (Mkn421, PKS2155-304) are rapidly variable sources, with complex flux-dependent spectral variability. Chandra and XMM-Newton CCD observations of these objects are almost invariably affected by pileup due to the better spatial resolution of their telescopes, higher effective area, and/or frame exposure time. For this reason, Chandra observes Mkn421 and PKS2155-304 only with the gratings to cut down the flux in the zero-order image. Mitigation actions in grating-less observations (such as those obtained with the EPIC) involve excising the PSF core from the spectral accumulation region, yielding additional uncertainties in the spectral deconvolution due to the possible energy dependence of the encircled energy fraction in the PSF wings.²⁶ Serendipitous catalogs for effective area calibration and cross-calibration have been alternatively used.^{27,28}

Plerionic spectra in pulsar wind nebulae (PWN) may represent a promising alternative. (In addition to the Crab, still used for the calibration of instrument sensitive above 10 keV such as the RXTE/PCA, and the NuSTAR instruments, see Table 4, and the instruments on-board MAXI, among others.) They are appropriate for calibration purposes due to their stability on human time scales and their simple nonthermal shape (often very well approximated, within the statistical quality of currently available x-ray measurements, by power-laws). The IACHEC study on G21.5-0.9²⁹ is currently the largest published

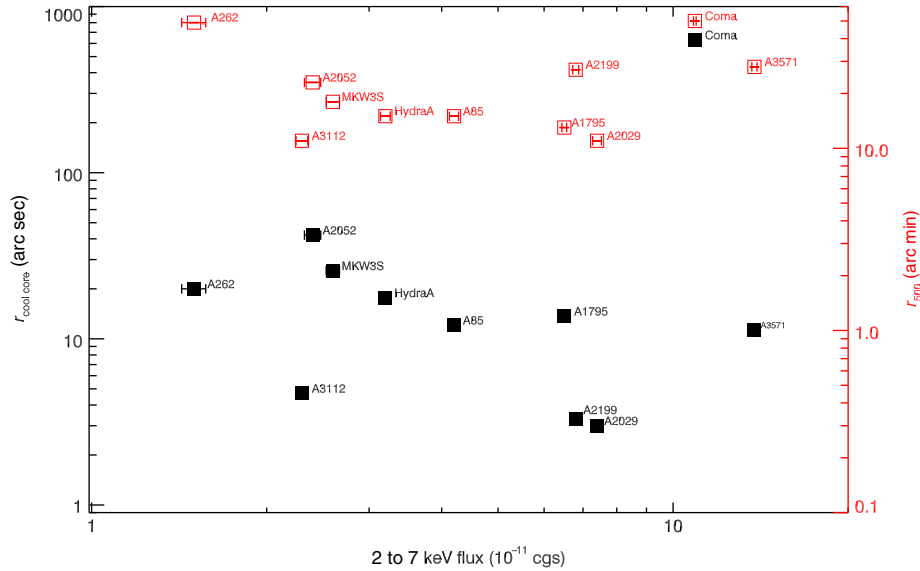


Fig. 3 Radii of the cool core (r_{coolcore} , filled squares, left y-axis), and r_{500} (empty squares, right y-axis) as a function of the 2 to 7 keV flux within 10 arc min for the sample of galaxy cluster after Nevalainen et al.³³

cross-calibration study ever in terms of number of instruments involved, covering the whole energy band from 2 to 150 keV (the source is obscured by a column density $\simeq 2 \times 10^{22} \text{ cm}^{-2}$). On the other hand, even a comparatively compact PWN as G21.5-0.9 ($\sim 3'$ size, with a central symmetric plerionic core of $\sim 30''$) may exceed the field-of-view of a narrow-field instrument, such as the future high-resolution microcalorimeter on-board ASTRO-H.

4.2 Molecular Contamination

Several missions have discovered after launch a buildup of molecular contamination on cold surfaces within the light path of their instruments.^{30,31} This contaminant absorbs x-ray photons at soft energies ($\lesssim 1 \text{ keV}$), and as it builds up, the effective area becomes a sensitive but uncertain function of time, location on the detector, and energy.

Measuring and modeling the temporal, spatial, and chemical characteristics of contaminants have proven to be challenging. Regular Chandra observations of bright continuum sources such as Mkn 421 with the gratings have been invaluable in measuring absorption edges and constraining the chemical composition of the contaminant building up on the ACIS filter. Off-axis pointing on Abell 1795 has monitored the spatial dependence (see Sec. 4.3). On the Suzaku/XIS, a large amount of contaminant built-up very quickly on the optical blocking filter in the first months of the mission, and early and frequent observations of soft, stable sources like 1E0102-72.3 and RXJ1856-6-3754 have been crucial in constraining its on-axis temporal dependence. Observations of the Cygnus Loop and the bright limb of the earth, which produces field-filling N-K and O-K emission lines, have helped to understand the spatial distribution. The location of the contaminant along the optical path to the EPIC-MOS camera is still unclear.

4.3 On Galaxy Clusters as Calibration Sources

Galaxy clusters have been extensively used as calibration sources because they are stable on human time scales. This

implies that the sufficiently hot clusters can be used at any time for any hard x-ray detector calibration observation and can be compared with observations taken in other epochs by the same or other detectors. Thus, large cluster samples can be formed for cross-calibration purposes without the considerable efforts involved in simultaneous cross-mission observation campaigns of variable sources. The largest sample of cross-calibration targets so far is that about 50 HIFLUGCS galaxy clusters.³² The nearest clusters hotter than about 6 keV are bright and hard, thus yielding sufficient photons for calibration experiments within typical standard x-ray calibration experiments' duration (a few hours). However, due to their surface brightness distribution, they are not too bright to produce pileup in CCD detectors. Also, PSF effects can be minimized by extracting data from regions larger than the size of the PSF. The combination of these factors makes galaxy clusters very suitable targets for effective area shape calibration.

In Fig. 3, we show the radius of the cluster cool core (r_{coolcore}) and r_{500} as a function of the 2 to 7 keV flux for the 11 objects of the Nevalainen et al.³³ galaxy cluster sample (see also Sec. 8).

The cool core clusters are preferred over the noncool core clusters, since the latter usually are mergers and have a very complex temperature structure, while the cool core clusters are typically relaxed and have isothermal structure at a radial range of 0.1 to $0.3 \times r_{500}$. On the other hand, Coma is very bright and, while being a noncool-core cluster, is rather isothermal in the inner region. Furthermore, using the stacking residuals ratio technique for the investigation of the effective area calibration uncertainties^{28,34,35} allows one to use almost any cluster notwithstanding its detailed thermal structure.

The only significant line emission in clusters hotter than 6 keV is due to recombination transitions from Fe_{XXV} and Fe_{XXVI} . The energy band covered by these lines ($\simeq 6.67$ to 6.96 keV) is narrow. The dependence of the effective area on energy in this energy range is smooth and shallow. This allows decoupling of the energy redistribution and effective area calibration effects. However, the extended nature of the x-ray emission in clusters is, at the same time, a curse and a blessing. It

causes different sky areas to be covered by different detectors. This requires additional exposure map corrections, known with different degrees of uncertainties in different detectors.

Abell 1795 has been used to monitor the spatial distribution of the contaminant in ACIS. At the same time, galaxy clusters have assumed the role of reference “standard candles” in the 2 to 10 keV band, following the pioneer cross-calibration work by Nevalainen et al.³³ using a sample covering a wide range of temperatures (2 to 10 keV), fluxes (0.3 to 4×10^{-11} erg cm⁻² s⁻¹ in the 2 to 7 keV energy band), and morphologies (Fig. 3). These authors found that the gas temperature in clusters of galaxies derived from the 2 to 6 keV continuum emission is in good agreement with that derived from the H- to He-like Fe line ratio for the EPIC cameras (see, e.g., Fig. 10 in Nevalainen et al.³³). This method requires a very large number of photons in the narrow range and has so far encountered limited application with real data due to the very deep exposures needed. It opens, however, promising perspectives for future high-resolution detectors at the Fe transition energies, such as the microcalorimeters on board ASTRO-H.

5 Effective Area at Energies >10 keV

Most of the operational instruments >10 keV (“hard x-ray band” hereafter) have employed the Crab Nebula as the primary calibrator for the effective area. The responses of the INTEGRAL/IBIS, RXTE/PCA,³⁶ and NuSTAR have been calibrated solely based on the Crab, assuming “standard values” for the photon index and normalization of a power-law shape. Weisskopf et al.³⁷ showed that some models of the nebula high-energy emission predict a spectral curvature that should already be measurable by the PCA. This evidence challenges the assumption underlying the calibration of its response. The status of the Crab Nebula as “the standard candle of x-ray astronomy” has been severely undermined; however, by two circumstances: (a) the fact that most instruments operating <10 keV during the first decade of the 21st century could not observe the Crab due to telemetry or pileup limits, except in special, rarely used instrumental modes; (b) the discovery that the Crab is actually a variable source^{38,39} exhibiting variations with a dynamical range of $\simeq 7\%$ over the whole x-ray band on time scales of months (a discovery delayed by the assumption that the Crab Nebula was a stable calibration source!).

Alternative plerionic spectra such as G21.5-0.9²⁹ and MSH15-52^{40,41} could yield a statistical accuracy on the determination of the spectra shape of $\Delta\Gamma \sim 0.05$ in a 50 ks observation with the hard x-ray focusing telescopes on NuSTAR and ASTRO-H. With a NuSTAR observation of 280 ks of G21.5-0.9, the error on the spectral index ($\Delta\Gamma \simeq 0.013$ ⁴²) is comparable to the systematic error due to uncertainties in the effective area calculations.⁴³ This level of statistical accuracy is sufficient to characterize the systematic uncertainties on the effective area intercalibration that are of the order $\Delta\Gamma \simeq 0.2$.²⁹ Recently, however, an observation by NuSTAR revealed the presence of a break in the spatially integrated spectrum of G21.5-0.9,⁴² with the spectral index going from 1.996 to 2.093 across a break at about 9.7 keV. This may eventually explain the systematically higher spectral indices measured at energies higher than 10 keV.²⁹ Comparable statistical quality could be obtained on bright radio-loud hard AGN such as 3C273⁴⁴ or Centaurus A.⁴⁵ However, 3C273 exhibits a hard x-ray flux historical variability of about 50%,⁴⁴ and Centaurus A is also a variable source.

In summary, no source is an ideal effective area calibrator in the hard x-ray band. It is recommendable to compile and compare measurements from different sources in order to achieve a good understanding of the hard x-ray effective area, e.g., the discussion in Madsen et al.,⁴³ and/or coordinated observations with other observatories to normalize the flux.

Typical observed spectra >10 keV for the sources discussed in this section are shown in Fig. 4.

6 Point Spread Function

“First-light”-like bright sources such as x-ray binaries (CygX-1, CygX-2, and HerX-1), stars (AR Lac, Capella) or bright AGN (3C273, MCG-6-30-15) have been used for this purpose, depending on the brightness limitations. Appropriate galactic sources need to be seen through a low absorbing column density to keep the possible broadening due to galactic dust scattering⁵⁰ to a level smaller than the calibration uncertainties. Obscured extra-galactic sources (AGN) could be a potentially promising alternative. However, they have not been considered as primary targets due to their comparative faintness. The main goal of these calibration experiments is measuring the wings to high precision. Since the contrast of wings to peak can be of several orders of magnitude, one needs typically $\sim 10^6$ counts or more to perform such measurements at the required level of accuracy (typically a few percent). The PSF core can be calibrated by stacking serendipitous sources.²⁶

Since significant pileup is encountered in ACIS observations of bright point sources, the Chandra team has generated a composite on-axis PSF from HRC-I observations of Ar Lac and Capella and an ACIS observation of Her X-1.⁵¹⁻⁵³ The Ar Lac and Capella data are used to measure the inner and outer core of the on-axis PSF, respectively, while the ACIS observation of Her X-1 (which is heavily piled-up) is used to measure the wings of the PSF. Her X-1 is a bright point source with a low column density and no dust halo. These three observations are renormalized to produce the on-axis PSF from 0.5” to 10’. Both the on-axis and off-axis PSF are measured and monitored by yearly HRC-I raster scans of AR Lac.

7 Timing

The preparation of an in-flight timing calibration plan requires observing pulsars and x-ray bursters covering a wide range of periods. This allows covering the different elements contributing to the accuracy of the event time stamping (delays, dead time, etc.). For Suzaku (In this context, it is interesting to note that the data acquisition system of ASTRO-H uses the standard network protocol SpaceWire able to assign a time stamp based on a global positioning system.) and XMM-Newton radio ephemeris are more accurate than x-ray ephemeris by 1 to 3 orders of magnitude, providing the required reference.^{54,55} In the case of timing x-ray observatory RXTE, the bulk of the error budget on the absolute timing is due instead to uncertainties in the radio ephemeris due to the interstellar scattering as well as to imperfect delays and polarization calibration.⁵⁶ At the shortest period range, the Crab pulsar ($\simeq 33$ ms) has been the main target used for both absolute and relative timing calibration.^{54,55} Alternative targets have been: A0535-262 (103 s), AE Aqr (33 s), Am Her (11140 s), Her X-1 (1.237 s), PSR B0540-69 (51 ms), PSR J0537-69 (50 ms), PSR B1055-52 (197 ms), PSR B1509-58 (in MSH15-52; 0.15135 s), and Vela pulsar (88 ms).

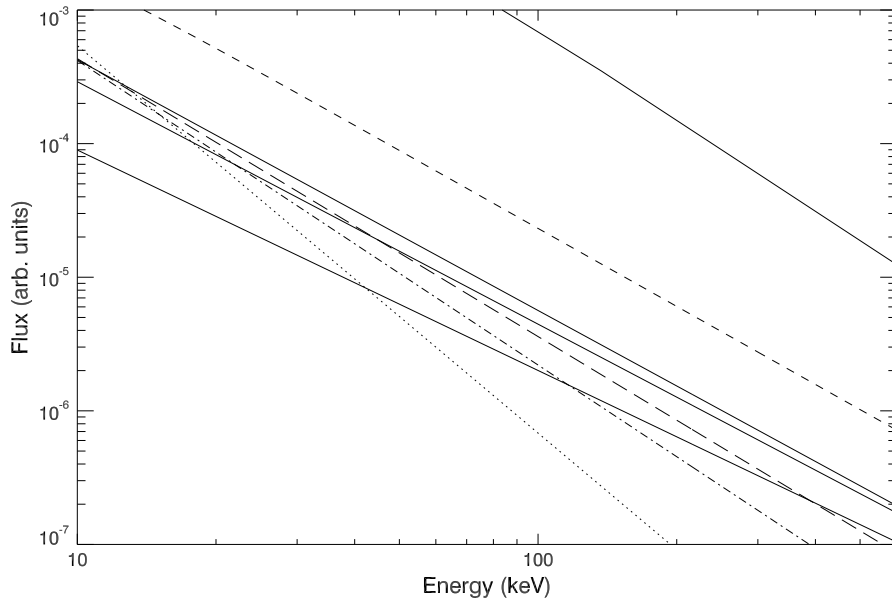


Fig. 4 Models of plerionic spectra above 10 keV to illustrate their relative intensity: Crab (top solid line);⁴⁶ G21.5-0.9 (dashed-dotted line);²⁹ and PSR1509-58 (dashed line).⁴¹ They are compared to the spectra of the SNR Cas A (dotted line),⁴⁷ and 3C273 in its lowest (lowest solid line) and highest (middle solid line) state in the 2003 to 2005 INTEGRAL and XMM-Newton monitoring,⁴⁸ and NGC 1275 (dashed-triple-dotted line), the AGN at the center of the Perseus cluster.⁴⁹

8 Cross-Calibration

Several IACHEC Working Groups¹, have been engaged in defining “standard candles” for cross-calibration purposes:

- Clusters of galaxies: Nevalainen et al.³³ discuss a sample of bright clusters of galaxies, used for the verification of the cross-calibration status among the ACIS, the EPIC,

and the BeppoSAX/MECS in the 0.7 to 10 keV energy band. The results of this study, later confirmed by Schellenberger et al.,³² stimulated and contributed to the recalibration of the Chandra effective area embedded in the CALDB change between version 3.4 and version 4.1 at the turn of this decade. Later this study was extended to the Suzaku/XIS,³⁵ contributing to the

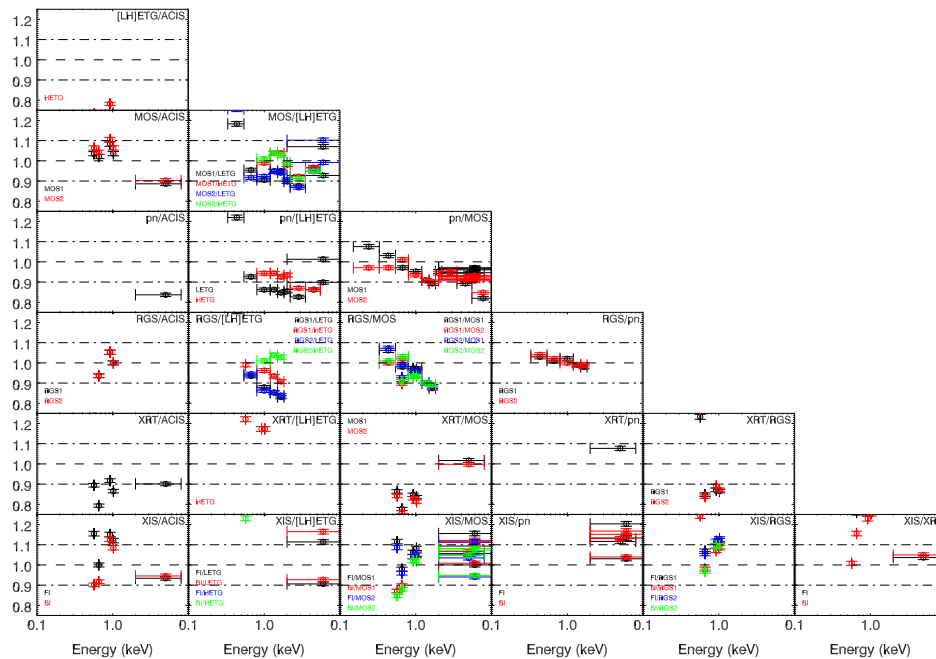


Fig. 5 Flux ratios as a function of energy in the 0.1 to 10 keV energy band for pairs of operational instruments compiled from IACHEC cross-calibration papers published in the last 3 years. The dashed lines correspond to the value of 1 on the y-axis (ideal perfect agreement); the dash-dotted lines correspond to $\pm 10\%$ around 1.

refinement of the calibration of the time evolution of their contamination layer. More recently this group has investigated the impact that cross-calibration uncertainties may have on the determination of the galaxy cluster mass and the consequent cosmological parameters through measurements of the intracluster gas temperature profile.^{32,57}

- Coordinated observations (already known as “effective area”): This WG has been running a cross-calibration campaign on PKS2155-304 since 2006.¹⁹ This campaign comprises simultaneous observations with Chandra, NuSTAR, Suzaku, Swift, and XMM-Newton (and now NuSTAR). Other blazars such as 3C273 and H1426+428 are the basis of a systematic comparison of the effective area calibration between the Chandra gratings and the XMM-Newton x-ray payload.⁵⁸
- Nonthermal SNR: This WG deals primarily with effective area cross-calibration >10 keV. This work has assumed additional importance as the pioneer work by Kirsch et al.⁵⁹ on the Crab Nebula has been challenged.^{39,37} An update of this study, solely based on quasisimultaneous observations, is being published.⁶⁰ As discussed in Sec. 5

alternative, albeit weaker, plerionic spectra have been proposed for this purpose, such as G21.5-0.9.²⁹

- Thermal SNR: The compact SNR 1E0102-72.3 has truly become a standard calibration target for redistribution, effective area, and contamination monitoring. A semiempirical model based on a continuum version of the APEC code⁶¹ was developed to describe its soft x-ray spectrum, and constrained observationally using the RGS spectra. The 1E0102-72.3 spectra are used to constrain the cross-calibration of the effective area at the energy of strong and well-isolated (at CCD resolution) He- and H-like transitions of OVII, OVIII, NeIX, and NeX.¹⁵
- White Dwarfs and INSs: The main goal of this WG is the refinement of the LETGS effective area in the softest x-ray energy band ($\lambda > 40$). Sources used for this purpose are WDs such as GD153, Hz43, and Sirius B, as well as the INS RXJ1856-6-3754.

Figure 5 represents a synopsis of cross-calibration measurements in the 0.1 to 10 keV energy band recently as published in IACHEC papers.^{15,19,29,35,33} It must be stressed that these results

Table 5 Sources used in IACHEC cross-calibration papers. Legend: “N10” = Nevalainen et al.;³³ “I11” = Ishida et al.;¹⁹ “T11” = Tsujimoto et al.;²⁹ “P12” = Plucinsky et al.;¹⁵ and “K13” = Kettula et al.³⁵ The over 50 galaxy clusters in Schellenberger et al.³² are not listed.

Source	ACIS	EPIC	LETG	ISGRI	MECS	PCA	RGS	XIS	XRT
1E0102-72	P12	P12					P12	P12	P12
Abell 1060		K13						K13	
Abell 1795	N10	N10,K13			N10			K13	
Abell 2029	N10	N10			N10				
Abell 2052	N10	N10							
Abell 2199	N10	N10			N10			K13	
Abell 262	N10	N10,K13							
Abell 3112	N10	N10,K13						K13	
Abell 3571	N10	N10			N10				
Abell 496		K13						K13	
Abell 85	N10	N10			N10				
AWM7		K13						K13	
Centaurus cluster		K13						K13	
Coma cluster	N10	N10,K13			N10			K13	
G21.5-0.9	T11	T11		T11		T11		T11	T11
Hydra A	N10	N10							
MKW3S	N10	N10							
Ophiucus cluster		K13						K13	
PKS2155-304		I11	I11					I11	
Triangulum cluster		K13						K13	

were published at different times, and thus do not correspond to a homogeneous set of calibrations. Readers are warmly encouraged to refer to the continuously updated IACHEC publication¹, for a discussion of the most updated cross-calibration status.

The status of intercalibration among operational instruments in three energy bands: “soft” ($E < 2$ keV), “medium” ($E \simeq 2$ to 10 keV), and “hard” ($E > 10$ keV) can be summarized as follows:

- **Soft:** Energy-dependent cross-calibration discrepancies in this energy band were reported by Nevalainen et al.³³ and Schellenberger et al.³² Recent results confirm that the ratio between the Chandra/ACIS and XMM-Newton/EPIC-pn fluxes increases from -10% to $+10\%$ going from 0.5 to 2 keV.⁶² A similar behavior is observed when comparing Swift/XRT and XMM-Newton/EPIC-pn. On the other hand, the flux ratio between the Suzaku/XIS and XMM-Newton/EPIC-pn cameras was shown to be energy-independent, and comprised between -5% and -10% ,³⁵ although a more recent and extensive study challenges these conclusions.⁶² A study on a sample of serendipitous sources extracted from the 2XMM catalog⁶³ showed that XMM-Newton/EPIC-MOS cameras yield fluxes which are, on the average, in good agreement with EPIC-pn.²⁸
- **Medium:** A generally good agreement is shown among all the operational CCD within $\pm 5\%$ in flux and spectral shape.³³
- **Hard:** Swift/BAT yields fluxes $\simeq 20\%$ lower than INTEGRAL/SPI. Spectral indices are in excellent mutual agreement (± 0.04),²⁹ however, NuSTAR (not operational at the time of the Tsujimoto et al.²⁹) also yields fluxes in agreement within a few percent when compared to the Suzaku/HXD.

Table 5 lists the sources used in IACHEC cross-calibration papers.

9 Summary and Conclusions

The main goal of this paper is to describe the variety of celestial sources used to calibrate x-ray space instrumentation. An inevitably sketchy description of the rationale behind their choice over the long history of x-ray astronomy accompanies the enumeration of this variety. While in principle calibration of space instruments should be fundamentally based on a complete physical model of the detector as well as of the collimator or telescope in front of them, various constraints during mission development may impose complementing or verifying the ground-based measurements with observations of celestial sources. The possible degradation of the instrument performance in the harsh space radiation environment may further shift the balance toward the need for a comprehensive set of in-flight calibration observations.

Unfortunately, the x-ray sky does not offer “standard candles” *strictu sensu*, i.e., sources whose absolute flux can be accurately estimated once spectral properties can be determined even in nonphotometric conditions. For most x-ray sources, we must be content with an educated guess of the physical processes responsible for their plasma emission. For this reason, absolute flux calibration is often more challenging than spectral calibration.

On the programmatic side, the experience of running in-flight calibration programs of large and complex observatories, analyzing the in-flight calibration data, and providing calibration products to an ever-growing community of x-ray astronomers suggest the following guidelines that future x-ray observatories like ASTRO-H and Athena may consider in the planning of their ground segment developments:

- For the sake of planning the calibration observational program and the calibration data analysis activities, one should conceive the whole scientific payload of a mission as a single instrument.
- Adequate resources should be allocated to accumulate sufficient ground-based data. In operational terms, “sufficient” here means “adequate to characterize the physical model of each instrument (telescope/collimator + detector system) within the accuracy requirements defined *a priori* on the basis of the main scientific objectives of the mission.” This remains true even if a recalibration might be required in space due to the changing environment and instrument performance after launch.
- Efforts should not be spared to make sure that basic ground-based data necessary for the production of calibration files are properly documented and stored in a common mission database. Ideally this database, as well as the software accessing and analyzing the data, should be seamlessly integrated in the calibration database and software package to be used for the analysis of scientific data.
- The teams responsible for the analysis of the calibration data and for the production of the calibration files should involve scientists from all of the instruments. Otherwise stated, the cross-calibration perspective has to be integrated as early as possible in the calibration work of each individual instrument.
- Calibration teams shall have immediate access to all the data in the science archive for calibration purposes, even for those missions where science data are covered by a proprietary period.

The scientific payload of each mission is a unique combination. Blindly applying past experience can only yield disaster. However, time in orbit is a precious commodity. If this paper triggers studies and decisions that will permit a more efficient use of the limited time allocated to calibration observations, therefore allowing a mission to produce more and better science for the same budget, it will have reached its primary objective.

Appendix: List of Instruments Discussed in this Paper

- AGILE: Astro-rivelatore Gamma a Immagini LEggero.⁶⁴
- BeppoSAX: Medium Energy Concentrator Spectrometer (MECS).⁶⁵
- Chandra: Advanced CCD Imaging Spectrometer (ACIS),⁶⁶ Low-Energy Transmission Grating (LETG),⁶⁷ High-Energy Transmission Grating (HETG),⁶⁸ High Resolution Camera (HRC).

- INTEGRAL: Soft INTEGRAL Gamma-ray Imager (IBIS/ISGRI),⁶⁹ Spectrometer on Integral (SPI),⁷⁰ Joint European x-ray Monitor (JEM-X).⁷¹
- MAXI: Gas Slit Camera (GSC),⁷² Solid-state Slit Camera (SSC).⁷³
- NuSTAR: Nuclear Spectroscopy Telescope Array (NuSTAR).⁴³
- RXTE: High-Energy x-ray Timing Experiment (HEXTE),⁷⁴ Proportional Counter Array (PCA).³⁶
- Suzaku: Hard x-ray Detector (HXD),⁷⁵ x-ray Imaging Spectrometer (XIS).³¹
- Swift: Burst Alert Telescope (BAT),⁷⁶ X-Ray Telescope (XRT).⁷⁷
- XMM-Newton: European Photon Imaging Camera (EPIC),^{78,79} Reflection Grating Spectrometer (RGS).⁸⁰

Acknowledgments

The IACHEC community is grateful to Marcus Kirsch (European Space Agency) and Steve Sembay (University of Leicester), without whose initiative, impulse, and enthusiasm the IACHEC would not exist. Their vision has revolutionized the way calibration of high-energy detectors is being carried out. J.N. acknowledges a PUT426 grant from the Estonian Research Council. The authors acknowledge detailed and stimulating reports from two anonymous referees that triggered significant changes in the original paper.

References

1. S. Sembay et al., “Defining high-energy calibration standards: IACHEC (International Astronomical Consortium for High-Energy Calibration),” in *American Institute of Physics Conf. Proc.*, Vol. 1248, pp. 193 (2010).
2. J. U. Ness et al., “Coronal density diagnostics with helium-like triplets: CHANDRA-LETGS observations of Algol, Capella, Procyon, Epsilon Eri, Alpha Cen A&B, UX Ari, AD Leo, YY Gem, and HR 1099,” *Astron. Astrophys.* **394**, 911 (2002).
3. Kashyap and Posson-Brown, submitted for publication.
4. M. Audard et al., “Extreme-ultraviolet flare activity in late-type stars,” *Astrophys. J.* **541**, 396 (2000).
5. S. S. Lalitha and J. Schmitt, “X-ray activity cycle on the active ultra-fast rotator AB doradus A. implication of correlated coronal and photometric variability,” *Astron. Astrophys.* **559**, A119 (2013).
6. K. Mitsuda et al., “The x-ray microcalorimeter on the NeXT mission,” *Proc. SPIE* **7011**, 70112K (2008).
7. L. Barragán et al., “Suzaku observation of IGR J16318-4848,” *Astron. Astrophys.* **508**, 1275 (2009).
8. F. Fürst et al., “Study of the many fluorescent lines and the absorption variability in GX 301-2 with XMM-Newton,” *Astron. Astrophys.* **535**, A9 (2011).
9. J. Torrejón et al., “A Chandra survey of fluorescence Fe lines in X-ray binaries at high resolution,” *Astrophys. J.* **715**, 947 (2010).
10. S. Owocki and D. Cohen, “X-ray line profiles from parameterized emission within an accelerating stellar wind,” *Astrophys. J.* **559**, 1108 (2001).
11. K. Arnaud, R. Smith, and A. Siemiginowska, *Handbook of X-ray Astronomy*, Cambridge University Press, Cambridge, Massachusetts (2011).
12. C. P. de Vries et al., “Calibration sources for the soft x-ray spectrometer instrument on ASTRO-H,” *Proc. SPIE* **8443**, 844353 (2012).
13. P. Plucinsky et al., “The SMC SNR 1E0102.2-7219 as a calibration standard for x-ray astronomy in the 0.3–2.5 keV bandpass,” *Proc. SPIE* **7011**, 70112E (2008).
14. Plucinsky et al., in preparation.
15. P. Plucinsky et al., “Cross-calibration of the x-ray instruments onboard the Chandra, Suzaku, Swift, and XMM-Newton observatories using the SNR 1E 0102.2-7219,” *Proc. SPIE* **8443**, 844312 (2012).
16. V. Burwitz et al., “The thermal radiation of the isolated neutron star RX J1856.5-3754 observed with Chandra and XMM-Newton,” *Astron. Astrophys.* **399**, 1109 (2003).
17. N. Sartore et al., “Spectral monitoring of RX J1856.5-3754 with XMM-Newton: analysis of EPIC-pn data,” *Astron. Astrophys.* **541**, A66 (2012).
18. K. K. Madsen et al., “3C 273 with NuSTAR: unveiling the active galactic nucleus,” *Astrophys. J.* **812**, 14 (2015).
19. M. Ishida et al., “Cross spectral calibration of Suzaku, XMM-Newton, and Chandra with PKS 2155-304 as an activity of IACHEC,” *Publ. Astron. Soc. Jpn.* **63**, 657 (2011).
20. S. Sembay, R. Saxton, and M. Guainazzi, “A phenomenological approach to calibrating the EPIC-MOS detector response,” in *The X-ray Universe 2011*, J. U. Ness and M. Ehle, Eds., 283 (2011).
21. K. Beuermann, V. Burwitz, and T. Rauch, “Establishing HZ43 A, Sirius B, and RX J185635-3754 as soft X-ray standards: a cross-calibration between the Chandra LETG+HRC-S, the EUVE spectrometer, and the ROSAT PSPC,” *Astron. Astrophys.* **458**, 541–552 (2006).
22. D. Patnaude et al., “A decline in the nonthermal X-ray emission from Cassiopeia A,” *Astrophys. J.* **729**, L28 (2011).
23. P. Grandi and G. C. Palumbo, “Jet and accretion-disk emission untangled in 3C 273,” *Science* **306**, 998–1002 (2004).
24. K. L. Page et al., “XMM-Newton observations of 3C 273,” *Mon. Not. R. Astron. Soc.* **349**, 57–67 (2004).
25. H. L. Marshall et al., “An X-ray imaging survey of Quasar jets: testing the inverse Compton model,” *Astrophys. J. Suppl. Ser.* **193**, 15 (2011).
26. A. Read et al., “A new comprehensive 2D model of the point spread functions of the XMM-Newton EPIC telescopes: spurious source suppression and improved positional accuracy,” *Astron. Astrophys.* **534**, A34 (2011).
27. S. Mateos et al., “Statistical evaluation of the flux cross-calibration of the XMM-Newton EPIC cameras,” *Astron. Astrophys.* **496**, 879 (2009).
28. A. Read, M. Guainazzi, and S. Sembay, “Cross-calibration of the XMM-Newton EPIC pn and MOS on-axis effective areas using 2XMM sources,” *Astron. Astrophys.* **564**, A75 (2014).
29. M. Tsujimoto et al., “Cross-calibration of the X-ray instruments onboard the Chandra, INTEGRAL, RXTE, Suzaku, Swift, and XMM-Newton observatories using G21.5-0.9,” *Astron. Astrophys.* **525**, A25 (2011).
30. H. Marshall et al., “Composition of the Chandra ACIS contaminant,” *Proc. SPIE* **5165**, 497–508 (2004).
31. K. Koyama et al., “X-ray imaging spectrometer (XIS) on board Suzaku,” *Publ. Astron. Soc. Jpn.* **59**, 23 (2007).
32. G. Schellenberger et al., “XMM-Newton and Chandra cross-calibration using HIFLUGCS galaxy clusters. Systematic temperature differences and cosmological impact,” *Astron. Astrophys.* **575**, A30 (2015).
33. J. Nevalainen, J. David, and M. Guainazzi, “Cross-calibrating X-ray detectors with clusters of galaxies: an IACHEC study,” *Astron. Astrophys.* **523**, A22 (2010).
34. A. L. Longinotti et al., “FERO (finding extreme relativistic objects): statistics of relativistic broad Fe K α lines in AGN,” in *Revista Mexicana de Astronomía y Astrofísica Conference Series*, Vol. 32, pp. 62–64 (2008).
35. K. Kettula, J. Nevalainen, and E. Miller, “Cross-calibration of Suzaku/XIS and XMM-Newton/EPIC using galaxy clusters,” *Astron. Astrophys.* **552**, A47 (2013).
36. N. Shaposhnikov et al., “Advances in the RXTE proportional counter array calibration: nearing the statistical limit,” *Astrophys. J.* **717**, 59 (2012).
37. M. Weisskopf et al., “On calibrations using the Crab Nebula and models of the nebular X-ray emission,” *Astrophys. J.* **713**, 912 (2010).
38. C. Greiveldinger and B. Aschenbach, “Temporal variability of the X-ray emission of the Crab Nebula torus,” *Astrophys. J.* **510**, 305 (1999).
39. C. Wilson-Hodge et al., “When a standard candle flickers,” *Astrophys. J.* **727**, L40 (2011).
40. D. Marsden et al., “The X-ray spectrum of the plerionic system PSR B1509-58/MSH 15-52,” *Astrophys. J.* **491**, L39 (1997).
41. T. Mineo et al., “The hard X-ray emission from the complex SNR MSH 15-52 observed by BeppoSAX,” *Astron. Astrophys.* **380**, 695 (2001).

42. M. Nynka et al., “NuSTAR study of hard X-ray morphology and spectroscopy of PWN G21.5-0.9,” *Astrophys. J.* **789**, 72 (2014).
43. K. Madsen et al., “Calibration of the NuSTAR high energy focusing x-ray telescope,” *ApJS* **220**, 8 (2015).
44. S. Soldi et al., “The multiwavelength variability of 3C 273,” *Astron. Astrophys.* **486**, 411 (2008).
45. Y. Fukazawa et al., “Suzaku view of x-ray spectral variability of the radio galaxy Centaurus A: partial covering absorber, reflector, and possible jet component,” *Astrophys. J.* **743**, 124 (2011).
46. T. Kouzu et al., “Spectral variation of hard x-ray emission from the Crab Nebula with the Suzaku Hard X-ray Detector,” *Publ. Astron. Soc. Jpn.* **65**, 74 (2013).
47. J. Vink et al., “The hard x-ray emission and 44ti emission of Cas A,” *Adv. Space Res.* **25**, 689 (2000).
48. M. Chernyakova et al., “2003–2005 integral and XMM-Newton observations of 3c 273,” *Astron. Astrophys.* **465**, 147 (2007).
49. D. Eckert and S. Paltani, “INTEGRAL observations of the Perseus cluster,” *Astron. Astrophys.* **495**, 415 (2009).
50. P. Predehl and J. Schmitt, “X-raying the interstellar medium: ROSAT observations of dust scattering halos,” *Astron. Astrophys.* **293**, 889 (1995).
51. P. Zhao and L. van Speybroeck, “A new method to model x-ray scattering from random rough surfaces,” *Proc. SPIE* **4851**, 124–139 (2003).
52. D. Jerius, T. Geatz, and M. Karovska, “Calibration of Chandra’s near on-axis optical performance,” *Proc. SPIE* **5165**, 433–444 (2004).
53. T. Geatz et al., “Calibrating the wings of the Chandra PSF,” *Proc. SPIE* **5165**, 411–422 (2004).
54. Y. Terada et al., “In-orbit timing calibration of the hard x-ray detector on board Suzaku,” *Publ. Astron. Soc. Jpn.* **60**, 25 (2008).
55. A. Martin-Carrillo et al., “The relative and absolute timing accuracy of the EPIC-pn camera on XMM-Newton, from x-ray pulsations of the Crab and other pulsars,” *Astron. Astrophys.* **545**, A126 (2012).
56. A. H. Rots, K. Jahoda, and A. G. Lyne, “Absolute timing of the Crab Pulsar with the Rossi x-ray Timing Explorer,” *Astrophys. J. Lett.* **605**, L129–L132 (2004).
57. H. Israel et al., “Reconciling Planck cluster counts and cosmology? Chandra/XMM instrumental calibration and hydrostatic mass bias,” *Mon. Not. R. Astron. Soc.* **448**, 814 (2015).
58. Smith and Marshall, in preparation.
59. M. Kirsch et al., “Crab: the standard x-ray candle with all (modern) x-ray satellites,” *Proc. SPIE* **5898**, 589803 (2005).
60. Natalucci et al., in preparation.
61. A. Foster et al., “Updated atomic data and calculations for x-ray spectroscopy,” *Astrophys. J.* **756**, 128 (2012).
62. Nevalainen et al., in preparation.
63. M. G. Watson et al., “The XMM-Newton serendipitous survey. V. The second XMM-Newton serendipitous source catalogue,” *Astron. Astrophys.* **493**, 339–373 (2009).
64. M. Tavani et al., “The AGILE mission,” *Astron. Astrophys.* **502**, 995–1013 (2009).
65. G. Boella et al., “The medium-energy concentrator spectrometer on board the BeppoSAX x-ray astronomy satellite,” *Astron. Astrophys. Suppl. Ser.* **122**, 327–340 (1997).
66. G. P. Garmire et al., “Advanced CCD imaging spectrometer (ACIS) instrument on the Chandra x-ray observatory,” *Proc. SPIE* **4851**, 28–44 (2003).
67. P. Predehl et al., “X-ray calibration of the AXAF low energy transmission grating spectrometer: effective area,” *Proc. SPIE* **3113**, 172–180 (1997).
68. C. R. Canizares et al., “The Chandra high-energy transmission grating: design, fabrication, ground calibration, and 5 years in flight,” *Publ. Astron. Soc. Pac.* **117**, 1144–1171 (2005).
69. P. Ubertini et al., “IBIS: the imager on-board INTEGRAL,” *Astron. Astrophys.* **411**, L131–L139 (2003).
70. G. Vedrenne et al., “SPI: the spectrometer aboard INTEGRAL,” *Astron. Astrophys.* **411**, L63–L70 (2003).
71. S. Brandt et al., “JEM-X inflight performance,” *Astron. Astrophys.* **411**, L243–L251 (2003).
72. M. Sugizaki et al., “In-orbit performance of MAXI gas slit camera (GSC) on ISS,” *Publ. Astron. Soc. Jpn.* **63**, 635 (2011).
73. H. Tomida et al., “Solid-state slit camera (SSC) aboard MAXI,” *Publ. Astron. Soc. Jpn.* **63**, 397–405 (2011).
74. D. E. Gruber et al., “The high energy x-ray timing experiment on XTE,” *Astron. Astrophys. Suppl.* **120**, C641–C644 (1996).
75. T. Takahashi et al., “Hard X-ray Detector (HXD) on board Suzaku,” *Publ. Astron. Soc. Jpn.* **59**, 35–51 (2007).
76. S. D. Barthelmy et al., “The burst alert telescope (BAT) on the SWIFT midex mission,” *Space Sci. Rev.* **120**, 143–164 (2005).
77. D. N. Burrows et al., “The Swift x-ray telescope,” *Space Sci. Rev.* **120**, 165–195 (2005).
78. L. Strüder et al., “The European photon imaging camera on XMM-Newton: the pn-CCD camera,” *Astron. Astrophys.* **365**, L18–L26 (2001).
79. M. J. L. Turner et al., “The European photon imaging camera on XMM-Newton: the MOS cameras: the MOS cameras,” *Astron. Astrophys.* **365**, L27–L35 (2001).
80. C. P. de Vries et al., “Calibration and in-orbit performance of the reflection grating spectrometer onboard XMM-Newton,” *Astron. Astrophys.* **573**, A128 (2015).

Biographies for the authors are not available.